The evolution of pyrrolizidine alkaloid diversity among and within Jacobaea species

Chen, Y.; Mulder, P.P.J.; Schaap, O.D.; Memelink, J.; Klinkhamer, P.G.L.; Vrieling K.

Research Article

The evolution of pyrrolizidine alkaloid diversity among and within *Jacobaea* species

Yangan Chen[1]* , Patrick P. J. Mulder[2], Onno Schaap[1], Johan Memelink[1], Peter G. L. Klinkhamer[1], and Klaas Vrieling[1]

[1]Institute of Biology, Leiden University, Sylviusweg 72, P. O. Box 9505, Leiden 2300 RA, The Netherlands
[2]RIKILT-Wageningen University & Research, Akkermaalsbos 2, P.O. Box 230, Wageningen 6700 AE, The Netherlands
*Author for correspondence. E-mail: y.chen@biology.leidenuniv.nl

Abstract Plants produce many secondary metabolites showing considerable inter- and intraspecific diversity of concentration and composition as a strategy to cope with environmental stresses. The evolution of plant defenses against herbivores and pathogens can be unraveled by understanding the mechanisms underlying chemical diversity. Pyrrolizidine alkaloids are a class of secondary metabolites with high diversity. We performed a qualitative and quantitative analysis of 80 pyrrolizidine alkaloids with liquid chromatography-tandem mass spectrometry of leaves from 17 *Jacobaea* species including one to three populations per species with 4–10 individuals per population grown under controlled conditions in a climate chamber. We observed large inter- and intraspecific variation in pyrrolizidine alkaloid concentration and composition, which were both species-specific. Furthermore, we sequenced 11 plastid and three nuclear regions to reconstruct the phylogeny of the 17 *Jacobaea* species. Ancestral state reconstruction at the species level showed mainly random distributions of individual pyrrolizidine alkaloids. We found little evidence for phylogenetic signals, as nine out of 80 pyrrolizidine alkaloids showed a significant phylogenetic signal for Pagel's λ statistics only, whereas no significance was detected for Blomberg's K measure. We speculate that this high pyrrolizidine alkaloid diversity is the result of the upregulation and downregulation of specific pyrrolizidine alkaloids depending on ecological needs rather than gains and losses of particular pyrrolizidine alkaloid biosynthesis genes during evolution.

Key words: ancestral state reconstruction, hierarchical cluster analysis, LC-MS/MS, phylogenetic signal, principal component analysis, secondary metabolite diversity.

1 Introduction

Plant secondary metabolites (SMs) are pervasive in the plant kingdom, functioning mainly as defense and/or signaling compounds (Wink, 2003; Moore et al., 2014). So far, more than 200 000 SMs have been isolated and identified (Kessler & Kalske, 2018), with being assigned to different compound classes including alkaloids, flavonoids, terpenoids, and glucosinolates. Within a given taxon, a single class of SM is commonly dominant. Within such a class, usually, a few major compounds are accompanied by several derivatives and minor related compounds (Wink, 2003). For example, in *Arabidopsis thaliana*, 34 different glucosinolates have been identified (Kliebenstein et al., 2001), and in the Lamiaceae, 147 terpenoids have been found (Mint Evolutionary Genomics Consortium, 2018). Besides the structural diversity, SMs often show remarkable quantitative variation. This is well documented for the abovementioned example of glucosinolates that showed about 20-fold difference in total concentrations among leaves of different ecotypes (Kliebenstein et al., 2001). As yet, due to their gigantic number and striking diversity, it is still an ongoing challenge to understand the cause behind this SM diversity and why such a large diversity is maintained in nature (Moore et al., 2014).

Aiming at untangling mechanisms behind SM diversity, researchers have put much effort in studying the distribution patterns of SMs under particular phylogenetic frameworks (Wink, 2003, 2008; Pelser et al., 2005; Courtois et al., 2015; Maldonado et al., 2017; Mint Evolutionary Genomics Consortium, 2018). Often, different classes of compounds emerge in an almost mutually exclusive manner in different taxa (Wink, 2003). For instance, glucosinolates are major SMs near-universally in the Brassicaceae, the Capparidaceae, and

the Caricaceae (Moore et al., 2014), whereas benzylisoquinoline alkaloids occur mainly in the Papaveraceae, the Ranunculaceae, the Berberidaceae, and the Menispermaceae (Ziegler & Facchini, 2008). Nevertheless, on a closer look within each chemical class, individual compounds can vary in presence and/or quantity in inconsistent ways with or without phylogenetic signals through a clade; however, members within the clade often share similar SMs (Pelser et al., 2005; Maldonado et al., 2017; Mint Evolutionary Genomics Consortium, 2018). This erratic distribution of particular SMs has puzzled botanists and ecologists for some time and has hindered the understanding of evolutionary origins of SM diversity. More dissections of SM diversity in a given chemical class under a particular phylogenetic context are needed.

Pyrrolizidine alkaloids (PAs) are a class of SMs with typical high diversity (Hartmann, 1996). More than 400 PAs existing as monoesters and open chain or macrocyclic diesters have been found in ca. 6000 angiosperm species (Chou & Fu, 2006), of which more than 95% belong to the Asteraceae, the Boraginaceae, the Fabaceae, and the Orchidaceae (Hartmann, 1999; Langel et al., 2011). Pyrrolizidine alkaloids of the macrocyclic senecionine type are especially diverse with more than 100 structures, which are characteristic for PA containing species of the tribe Senecioneae of the Asteraceae (e.g., the genus *Senecio*; Langel et al., 2011). In *Senecio*, senecionine *N*-oxide synthesized in roots (Hartmann & Toppel, 1987; Toppel et al., 1987) was identified as the backbone structure of most PAs (Hartmann & Dierich, 1998). Senecionine *N*-oxide is transported via the phloem to shoots, where PA diversification takes place (Hartmann et al., 1989), resulting in species-specific or ecotype-specific PA bouquets (Hartmann & Dierich, 1998). Pyrrolizidine alkaloids are present in plants as *N*-oxides and/or tertiary amines (free bases) (Wiedenfeld et al., 2008; Mulder et al., 2018), and in most cases, PAs are synthesized and stored in their polar salt-like *N*-oxide form (Langel et al., 2011).

All the *Jacobaea* species (26 species and formerly a part of *Senecio* species) produce PAs (Pelser et al., 2005; Langel et al., 2011), but the composition and concentration appear to be species-specific (Soldaat et al., 1996; Hartmann & Dierich, 1998; Langel et al., 2011). Besides interspecific variation, a large variety of PA profiles within species was found. Different chemotypes of *J. vulgaris* and *J. erucifolia* are good examples of this intraspecific variation (Witte et al., 1992; Macel et al., 2004). For example, chemotypes of *J. vulgaris* either possessed jacobine or erucifoline as the dominant PA (Witte et al., 1992). In a later study on *J. vulgaris*, a chemotype was found that lacked jacobine and erucifoline, but had senecionine as the dominant PA (Macel et al. 2004). The species in the genus *Jacobaea* have often been used to explore the evolutionary basis of SM diversity (Vrieling et al., 1993; Hartmann & Dierich, 1998; Macel et al., 2004; Cheng et al., 2011). Pelser et al. (2005) constructed the evolutionary history of qualitative PA variation (presence/absence of PAs) of herbarium samples of 24 *Jacobaea* species using GC/MS. Interestingly, they found only weak phylogenetic signals, as PA distribution appeared to occur largely incidentally within the whole clade. These authors suggested that PAs evolve and disappear rapidly during evolution.

In this study, we wanted to verify or falsify the results of these authors by using more rigid methods. Pelser et al. (2005) were restricted by the use of herbarium specimens rather than fresh plant samples. This may have led to unwanted structural transformations and breakdown of particular PAs (Sander & Hartmann, 1989). Furthermore, the herbarium specimens were field-collected and not grown under controlled circumstances. Most importantly, many species only had one specimen or a pooled sample due to the lack of enough material of single specimens. To show the absence of a phylogenetic signal and for a proper insight into the distribution of the expression of particular compounds, it is essential to investigate if the variation in expression within species is larger than the variation between species. In the present study, we used a more sensitive analytical method and performed both quantitative and qualitative analyses of 80 PAs with liquid chromatography-tandem mass spectrometry (LC-MS/MS) of 8–10-week old leaves from 17 *Jacobaea* species, each of which was represented by one to three populations with 4–10 individuals per population grown under controlled conditions. In addition, we amplified and sequenced 11 chloroplast DNA regions and three nuclear markers to fully resolve the molecular phylogeny of *Jacobaea* species. The resulting phylogenetic tree was used as a "roadmap" to trace the evolutionary histories and to explore phylogenetic signals present within PA distributions.

2 Material and Methods

2.1 Chemicals

Formic acid (analytical grade) and ammonium carbonate (analytical grade) were obtained from Sigma-Aldrich, Zwijndrecht, The Netherlands. Acetonitrile (LC–MS grade) and methanol (LC–MS grade) were obtained from Actu-all, Oss, The Netherlands. Twenty-seven PA analytical standards were available, which were sourced from Phytoplan (Heidelberg, Germany), except for heliotrine (Valence, France), usaramine (BOC Sciences, Shirley, NY, USA), and florosenine (Prisna, Leiden, The Netherlands). Usaramine *N*-oxide was in-house synthesized by reaction of usaramine with 30% hydroperoxide in methanol/water. Acetylerucifoline and acetylseneciphylline were prepared in-house from, respectively, erucifoline and seneciphylline, by acetylation with acetic anhydride and dimethylaminopyridine in toluene. See Additional file S1 for a full list of PA standards used in this study. Stocks in methanol (100 mg/L) of the individual standards were prepared. Aliquots (1 mL) of these stock solutions (except for heliotrine) were combined to prepare a mixed standard solution in methanol (4 mg/mL).

2.2 Plant material

Seeds were obtained from botanical gardens or commercial seed companies including 40 accessions (Table 1), representing 17 of the 26 *Jacobaea* species. Of the 40 accessions obtained, 34 were collected from known natural locations, whereas the location of collection was unknown for six accessions. The 17 chosen species are evenly distributed throughout the three main clades (i.e., *Incani* s.l. group, *J. vulgaris* s.l. group, and *J. paludosa* group), according to the phylogeny inferred by Pelser et al. (2004). Each *Jacobaea*

Table 1 Average PA concentrations (µg/g DW) in the leaves of each accession summed over PA groups of 17 *Jacobaea* species

Clade	Species /Accessions	Origins of seeds[‡]	Individuals	Total PAs Mean	Total PAs SE	Sum FB Mean	Sum FB SE	Sum NO Mean	Sum NO SE	sum Sn Mean	sum Sn SE	sum Jb Mean	sum Jb SE	sum Er Mean	sum Er SE	sum Pt Mean	sum Pt SE	sum Ot Mean	sum Ot SE	Sum unk Mean	Sum unk SE
Incani s.l. group	*J. abrotanifolia* 1	Austria[1]	5	62.1	7.7	58.4	7.2	3.7	1.8	1.3	0.4	0.0	0.0	5.5	1.9	0.0	0.0	55.2	7.0	0.0	0.0
	J. abrotanifolia 2[†]	Switzerland[2]	7	35.5	5.6	35.0	6.2	0.5	0.2	0.4	0.2	0.1	0.1	0.2	0.1	0.0	0.0	34.8	5.7	0.0	0.0
	J. abrotanifolia 3	Italy[3]	5	65.1	11.5	64.2	11.5	1.0	0.2	0.9	0.3	0.1	0.0	1.1	0.3	0.0	0.0	63.1	11.5	0.0	0.0
	J. adonidifolia 1[†]	Switzerland[2]	10	64.0	12.4	27.9	5.1	36.1	10.8	1.5	0.4	0.1	0.0	40.8	11.4	0.1	0.0	21.5	5.1	0.1	0.0
	J. adonidifolia 2[†]	Italy[3]	5	127.1	33.6	37.5	14.5	89.6	24.6	13.1	9.3	0.2	0.1	113.6	29.1	0.1	0.0	0.0	0.0	0.2	0.2
	J. adonidifolia 3	France[4]	10	211.3	35.2	132.7	23.4	78.5	13.2	20.0	8.4	0.3	0.1	65.5	8.0	0.1	0.0	124.4	22.2	1.0	0.4
	J. carniolia 1[†]	Italy[3]	2	652.0	312.2	252.4	78.3	399.6	233.9	518.8	280.3	0.4	0.3	82.0	24.8	12.8	6.9	5.6	1.7	32.4	1.7
	J. carniolia 2	Italy[3]	6	676.8	133.4	48.4	12.2	628.4	133.6	644.0	132.9	0.3	0.1	13.0	3.8	6.9	4.9	1.4	0.8	11.2	2.0
	J. carniolia 3	Italy[3]	6	44.8	5.9	19.4	2.0	25.4	5.9	29.2	5.7	0.0	0.0	5.1	2.4	2.0	1.6	6.8	2.2	1.6	0.4
	J. incana 1	Alps[5]	6	948.2	402.4	29.9	12.5	918.3	398.8	906.8	393.9	0.2	0.1	0.0	0.0	12.0	9.4	20.4	12.7	8.9	2.7
	J. incana 2	Switzerland[2]	8	1153.2	137.6	7.0	1.5	1146.2	136.3	1126.2	136.5	0.1	0.0	0.0	0.0	5.6	2.4	0.4	0.2	20.8	1.7
	J. incana 3	Switzerland[2]	7	1060.4	157.7	51.9	22.8	1008.5	145.6	991.7	144.6	0.1	0.0	0.0	0.0	7.7	2.2	39.2	22.0	21.8	2.7
	J. leucophylla 1	France[6]	4	84.2	50.9	5.4	2.2	78.7	50.9	74.4	50.7	0.0	0.0	0.0	0.0	1.2	0.4	2.8	2.2	5.7	1.5
	J. uniflora 1	Alps[5]	6	268.1	75.9	31.4	12.3	236.8	64.5	236.6	64.7	0.0	0.0	0.0	0.0	0.7	0.3	28.6	11.6	2.2	0.4
	J. uniflora 2	Switzerland[2]	5	538.0	72.0	202.1	56.0	335.9	37.0	332.7	36.9	0.0	0.0	0.0	0.0	2.7	0.8	196.5	56.0	6.1	0.6
J. vulgaris s.l. group	*J. alpina* 1	Alps[5]	9	2129.6	248.5	191.6	15.5	1938.0	235.9	1929.0	236.1	37.4	2.6	0.0	0.0	134.3	10.3	0.0	0.0	29.0	3.9
	J. alpina 2	France[6]	10	425.4	53.9	28.4	3.7	397.1	53.5	365.2	51.2	14.5	2.7	0.0	0.0	29.9	2.8	0.0	0.0	15.8	1.5
	J. alpina 3	Italy[7]	5	2133.8	259.7	1080.2	142.4	1053.6	190.8	1026.7	187.3	1.5	0.3	1.5	0.4	45.6	5.6	1050.4	142.0	8.1	1.2
	J. arnautorum 1	Bulgaria[8]	9	799.9	128.4	36.2	8.3	763.8	121.9	787.4	127.9	0.3	0.1	0.2	0.2	4.7	1.8	0.0	0.0	7.3	0.3
	J. subalpina 1	Slovakia[8]	10	1230.8	198.4	52.0	9.2	1178.8	190.7	1220.5	196.9	0.3	0.2	0.0	0.0	2.5	0.4	0.0	0.0	7.4	1.3
	J. subalpina 2	Austria[9]	9	2125.7	314.1	15.0	1.9	2110.7	312.3	2101.6	312.5	0.1	0.1	0.0	0.0	10.1	5.4	0.0	0.0	13.9	1.8
	J. subalpina 3	Slovakia[10]	7	672.6	107.3	9.2	1.5	663.4	106.7	663.9	106.5	0.0	0.0	0.0	0.0	1.5	0.5	0.0	0.0	7.2	1.0
	J. vulgaris 1	Germany[10]	5	1389.4	118.7	1105.6	103.0	283.8	62.1	71.5	20.2	1256.0	94.9	33.6	13.7	4.8	1.4	1.7	1.6	21.8	4.1
	J. vulgaris 2	UK[8]	5	4301.3	495.4	2994.9	483.9	1306.4	227.0	195.0	57.0	4053.5	480.7	20.8	6.1	7.7	3.5	0.0	0.0	24.2	5.4
	J. vulgaris 3	Netherlands[11]	5	3230.4	238.0	2905.0	181.2	325.5	65.3	91.9	23.5	2916.8	188.8	123.0	46.3	4.1	1.1	0.0	0.0	94.7	12.0
	J. aquatica 1	Germany[1]	10	1129.8	261.2	890.5	276.5	239.3	47.1	222.1	53.1	13.0	3.4	42.8	10.0	23.5	5.3	826.4	274.7	2.0	0.3
	J. aquatica 2	UK[8]	10	1412.7	160.3	253.5	35.5	1159.2	132.6	1124.5	130.0	24.9	2.3	4.3	4.1	89.9	11.1	166.3	31.0	2.8	0.2
	J. analoga 1	India[1]	10	368.1	67.3	172.9	31.6	195.2	61.4	182.2	62.5	154.4	21.3	0.0	0.0	27.2	7.3	0.0	0.0	4.3	0.8
	J. gnaphalioides 1	Greece[1]	10	3835.7	306.2	2461.4	126.9	1374.4	202.4	1246.6	203.8	113.0	30.2	0.0	0.0	1306.9	150.7	1101.8	101.1	67.5	13.6
	J. maritima 1	Alps[5]	7	516.0	82.1	343.3	57.0	172.7	59.3	80.1	28.1	433.0	70.3	0.0	0.0	0.2	0.1	0.0	0.0	2.8	0.7
	J. maritima 2	France[4]	5	1527.0	139.2	1390.8	139.3	136.2	42.3	185.8	77.0	1300.4	111.4	0.0	0.0	1.9	0.4	30.0	26.8	8.9	1.7
	J. maritima 3	Bulgaria[12]	5	1209.6	95.5	1046.3	120.1	163.2	29.6	29.3	5.2	1087.8	109.3	0.0	0.0	1.1	0.3	85.0	28.2	6.3	1.2
	J. erucifolia 1	Germany[10]	5	114.7	20.1	49.7	10.5	65.0	12.6	81.1	14.3	0.5	0.1	27.9	4.7	0.8	0.3	1.8	1.0	2.7	0.5
	J. erucifolia 2	UK[8]	6	288.8	83.1	32.9	11.7	255.9	75.2	219.7	67.7	1.2	0.5	62.5	17.5	1.0	0.5	1.5	0.6	2.9	0.8
	J. erucifolia 3	Netherlands[13]	5	22.3	6.1	5.7	2.2	16.6	4.5	18.9	5.8	0.1	0.0	2.3	0.0	0.0	0.0	0.6	0.3	0.4	0.2

Continued

Table 1 Continued

Clade	Species /Accessions	Origins of seeds[‡]	Individuals	Total PAs Mean	SE	Sum FB Mean	SE	Sum NO Mean	SE	sum Sn Mean	SE	sum Jb Mean	SE	sum Er Mean	SE	sum Pt Mean	SE	sum Ot Mean	SE	Sum unk Mean	SE
J. paludosa group	J. cannabifolia 1	Estonia[14]	5	6.2	1.1	4.7	1.1	1.6	0.3	1.2	0.3	4.2	0.8	0.6	0.4	0.0	0.0	0.1	0.0	0.0	0.0
	J. cannabifolia 2[†]	Italy[3]	7	9.2	7.2	8.6	7.0	0.6	0.2	3.1	2.7	2.5	2.0	3.3	2.4	0.1	0.1	0.0	0.0	0.1	0.1
	J. cannabifolia 3	Russia[15]	4	83.2	21.2	75.9	21.4	7.3	0.9	8.9	2.7	47.7	12.8	24.4	8.4	1.7	0.3	0.0	0.0	0.5	0.1
	J. paludosa 1	Poland[16]	5	127.4	36.0	121.6	34.7	5.7	2.2	4.6	2.2	0.1	0.0	0.0	0.0	0.0	0.0	121.4	34.7	1.2	0.3
	J. paludosa 2[†]	Germany[17]	4	149.9	26.8	80.2	14.9	69.7	22.8	51.2	18.7	86.8	13.2	0.0	0.0	8.3	2.9	0.0	0.0	3.6	1.0

[†]Seeds cultivated by the corresponding botanical garden with unknown exact origin in the wild; [‡]Seed donors/suppliers: [1]=Botanischer Garten und Botanisches Museum of Freie Universität Berlin, [2]=Conservatoire et Jardin botaniques de la Ville de Genève, [3]=Giardino Botanico Alpino Rezia, [4]=Jardin Botanique Alpin du Lautaret, [5]=B and T World Seeds, [6]=Jardins Botaniques du Grand Nancy et de l'Université de Lorraine, [7]=Giardino Botanico Daniela Brescia, [8]=Royal Botanic Garden Kew, [9]=Botanischer Garten des Institutes für Botanik der Universität Graz, [10]=Hortus Botanicus Leiden, [11]=Plant Ecology Group, Institute of Biology Leiden, [12]=Palace and Botanical Gardens of Balchik, [13]=Cruydt-Hoeck Wildeplantenzaden, [14]=Hortus Botanicus Tallinnensis, [15]=Botanical Garden-Institute FEB RAS, [16]=Polish Academy of Sciences Botanical Garden Center for Biological Diversity Conservation in Powsin, [17]= Botanical Garden of TU Braunschweig. Er, erucifoline-like; FB, free base; Jb, Jacobine-like; NO, N-oxide; Ot, otosenine-like; Pt, platyphylline-like; SE, standard error; Sp, seneciphylline-like; Sn, senecionine-like; Total PAs, sum of all PAs; Unk, unknown.

species contains one to three populations with 4–10 (average 6.6) individuals per population (Table 1). *Senecio vulgaris* that belongs to *Senecio* sect. *Senecio* was used as the outgroup for phylogenetic analyses only.

2.3 Plant growth and harvest
Seeds were germinated on the surface of a wet potting soil covered by plastic bags, and the seedlings were transferred into $9 \times 9 \times 10$ cm pots filled with 50% sandy soil (collected from Meijendel, The Netherlands), 50% potting soil (Slingerland Potgrond, Zoeterwoude, The Netherlands), and 1.5-g/L Osmocote slow release fertilizer (Scott, Scotts Miracle-Gro, Marysville, OH, USA; N: P: K = 15: 9: 11). Plants were kept in a climate room (humidity 70%, 16 h/8 h light/dark cycle at 20 °C). Two to five fully grown vegetative leaves or early stem leaves were harvested after eight or ten weeks. Leaves were ground into fine powder in liquid nitrogen. A part of the powder was stored at −80 °C until DNA extraction, and the rest was freeze-dried and stored at −20 °C until PA extraction (Cheng et al., 2011).

2.4 Preparation of extracts
The extraction protocol as described in the study of Cheng et al. (2011) was followed with some modifications. Ten milligrams of powdered plant material was extracted with 1 mL of 0.2% formic acid, which contained 1 μg/mL of heliotrine as an internal standard. After being shaken for 30 min on a tumbling machine, the extract was centrifuged at 13 000 rpm for 10 min and the supernatant was filtered through a 0.2-μm nylon membrane (Acrodisc 13-mm syringe filter; Pall Life Sciences, Ann Arbor, MI, USA). The filtered solutions were further diluted with milliQ water, depending on the expected concentrations in the extracts (see below). The additional dilution factor ranged from no dilution, in the case of *J. cannabifolia*, to 10-fold (*J. adonidifolia, J. erucifolia*), 25-fold (*J. abrotanifolia, J. analoga, J. carniolia, J. leucophylla, J. maritima, J. paludosa, J. uniflora*), and up to 50-fold dilution (*J. alpina, J. aquatica, J arnautorum, J. gnaphalioides, J. incana, J. subalpina, J. vulgaris*).

2.5 LC–MS/MS analysis
The analysis of PAs was performed on a LC–MS/MS system consisting of Waters Acquity ultra-performance liquid chromatography (UPLC) coupled to a Xevo TQ-S tandem mass spectrometer (Waters Corporation, Milford, MA, USA), running in a positive electrospray mode. Chromatographic separation was achieved on an Acquity BEH C18 analytical column, 150×2.1 mm, with 1.7-μm particle size (Waters Corporation). Eluent A consisted of water containing 10-mM ammonium carbonate (pH 9.0), and acetonitrile was used as eluent B. The gradient elution was performed as follows: 0.0 min 100% A/0% B, 0.1 min 95% A/5% B, 3.0 min 90% A/10% B, 7.0 min 76% A/24% B, 9.0 min 70% A/30% B, 12.0 min 30% A/70% B, 12.1–15.0 min 100% A/0% B. The column was kept at 50 °C and a flow rate of 400 μL/min was applied. Furthermore, 2-μL sample extract was injected. For each analyte, at least two selected precursors to product ion multiple reaction monitoring (MRM) transitions were measured. The cone energy was 40 V and collision energy settings were optimized for the individual compounds. Besides the 26 PAs, for which an analytical standard was

available, the samples were screened for another 54 PAs, for which no standards were available (see below). These PAs were included in the analytical method based on mass spectrometric data obtained from the analysis of extracts prepared from test samples of the individual *Jacobeae* species. See Additional file S1 for an overview of the MS/MS transitions used for the complete set of PAs.

2.6 Screening for new PA metabolites

The screening for new PA metabolites was conducted in the same way as described in detail in the study of Castells et al. (2014). Test samples of the *Jacobeae* species were extracted as described above, but no additional dilution was applied. The extracts were analyzed by running the LC–MS/MS in the parent ion scanning mode. Fragment ions typically present in the fragmentation spectra of a specific type of PA were selected: ions with m/z 94: 118, 120, and 138, indicative of senecionine-, jacobine-, and erucifoline-like PAs; ions with m/z 122: 150 and 168 for otosenine-like PAs; and ions with m/z 96: 122 and 140, typical for platyphylline-like PAs (These et al., 2013; Castells et al., 2014). When a parent ion (the protonated molecular ion) was present in two or more scans produced from different fragment ions, this ion was marked as a potential PA. Further analysis of these potential PAs was conducted by measurement of the complete fragmentation spectrum at different collision energies (typically 20–30–40 eV). Compounds that produced fragmentation spectra indicative for PAs were included in the MRM method. Where possible, a tentative assignment was made. In case this was not possible, the compound was annotated as either a free base compound or an *N*-oxide, including the protonated molecular mass and the retention time. A distinction between the free base and *N*-oxide form was made by measurement of the extract with and without chemical reduction (by adding a $Na_2S_2O_5$ solution to a part of the extract (Joosten et al., 2010, Castells et al., 2014). Compounds that upon reduction disappeared in the chromatogram were considered to be PA *N*-oxides, whereas compounds that remained stable or increased in concentration were considered to be PA free bases. In total, 54 PAs were tentatively identified in one or more of the plant extracts and these were included in the final MRM method. The test extracts were also used to determine the optimal dilution factor before LC–MS/MS analysis of the extracts of each species. Depending on the concentration of the PAs found in the test extracts, a dilution factor was estimated that was used to dilute the plant extracts. Dilution of most of the plant extracts was necessary to ensure that abundant PAs could be measured within the range of the standard calibration solutions. For the fragment ions, a peak area cut-off of 1000 was used. For each metabolite, retention times (± 0.02 min) and ion ratios ($\pm 30\%$) were compared with available standards, or in case of tentative metabolites, with the average retention time and ion ratio in the positive samples.

2.7 Quantification

The samples were run in a non-randomized order. Quantification was performed against a range of mixed standard solutions (0–5–10–25–50–100–200 µg/L) of the PAs in a diluted extract of *Tanacetum vulgare* (tansy). The extract of *T. vulgare* material was prepared in the same way as the other extracts and was used to mimic a PA-free plant extract. The range of

mixed standard solutions was injected at the beginning of the series and at the end. The mixed standard solution of 50 µg/L in *T. vulgare* extract was injected every 30–40 samples, to monitor the performance of the system (drift in retention time and changes in detector sensitivity) during the analysis. For each PA, the averaged response of two MRM transitions was used for quantification. For those compounds for which no reference standard was available, a semi-quantitative (indicative) value was obtained by comparison with the most closely related analog (e.g., an isomer). For metabolites with tentative or unknown structures, no closely related standard could be identified. In such cases, the concentration was estimated by taking the sum of the two most intense MRM transitions and comparing this with the sum area of a selected reference standard, as indicated in Additional file S1. Data processing was conducted with MassLynx 4.1 software (Waters Corporation).

2.8 Statistical analyses of metabolomics data

We performed analyses, quantitatively and qualitatively, using absolute concentrations, relative concentrations, and binary-coded presence (1)/absence (0) of all individual PAs of all *Jacobaea* plants (Additional file S1). Before any statistical analysis, the absolute and relative concentrations were log-transformed prior to Pareto scaling, and the binary data were also processed with the Pareto scaling method, but without prior transformation.

To extract and display the systematic variation of PA profiles, principal component analyses (PCA) were performed in SIMCA 15.0.2 and MetaboAnalyst (Chong et al., 2018). To compare similarities between PA profiles of different plant individuals, hierarchical cluster analyses (HCA) calculated with Euclidean distances and the Ward clustering algorithm were conducted using the tool MetaboAnalyst. We also performed Spearman rank correlation tests between all individual PAs using PA information extracted from all *Jacobaea* plants in MetaboAnalyst.

2.9 Phylogenetic analyses

DNA was extracted from leaf powder using the Qiagen DNeasy Plant Mini Kit. In total, 11 plastid regions and three nuclear regions were amplified and sequenced. Primers used for amplification and sequencing are listed in Table S1. PCR products were sequenced on both strands for each region for all species, whenever possible. Sequences were edited and assembled in Sequencher® version 5.0 DNA sequence analysis software (Gene Codes, Ann Arbor, MI, USA), and the resulting consensus sequences were aligned for each region using default parameters in MUSCLE implemented in MEGA7 (Kumar et al., 2016), followed by manual curation, where necessary. Gaps in the alignments were represented by the "-" character. Subsequently, individual alignments were concatenated using Sequence Matrix software (Vaidya et al., 2011) to generate a combined dataset. Missing data were represented by "?" character. The concatenated sequence of each species in the combined alignment is available in GenBank (accession numbers: MT396322-MT396339).

Phylogenetic analyses were conducted using maximum likelihood (ML), Bayesian inference (BI), and maximum parsimony (MP) algorithms. The ML tree was obtained through IQ-tree with automatic evolutionary model selection (Nguyen et al., 2015; Kalyaanamoorthy et al., 2017) on XSEDE

through CIPRES Science Gateway (http://www.phylo.org/). TIM + F + R2 was automatically chosen as the best-fit model according to the Bayesian Information Criterion. Bootstrap (BS) search was conducted using standard nonparametric bootstrap with 1000 replicates. BI was conducted with MrBayes 3.2.6 (Ronquist & Huelsenbeck, 2003), also on XSEDE through CIPRES Science Gateway. Two independent BI independent analyses were started simultaneously. The widely used GTRGAMMA substitution model, which assumes that the six substitution rates are independent gamma-distributed random variables with the same scale parameter, was used, as it is sufficient for a reliable phylogenetic inference (Abadi et al., 2019). The Markov Chain Monte Carlo analyses (Altekar et al., 2004) were run for 1 000 000 generations on four chains, sampling every 1000 generations. Twenty-five percent of the sampled values were discarded as burn-in when calculating the convergence diagnostics. The minimum frequency required for a partition to be included in the calculation of the topology convergence diagnostic was set to 0.1. The chain was stopped when the topological convergence diagnostic fell below the stop value of 0.001. The 50% majority-rule consensus tree was generated. Node support was assessed on the basis of Bayesian posterior probabilities (PP), where PP larger than 0.95 was considered as strongly supported. Furthermore, MP analyses were carried out using heuristic search in PAUP* 4.0a164 using 1000 replicates of random taxon addition sequence and the bisection-reconnection branch-swapping option. All characters were included in analyses and equally weighted, and gaps were treated as missing values. BS search of all combined datasets was performed with 1000 replicates. All resulting phylogenetic trees were visualized in FigTree version 1.4.4 (http://tree.bio.ed.ac.uk/software/figtree/).

2.10 Ancestral state reconstruction and phylogenetic signals
For chemical diversity ancestral state reconstruction, we used the Mk1 model (Lewis, 2001) developed for discrete morphological data. This model assumes that transition rates of both forward and backward changes are equal/symmetrical. Overall, the 80 PA compounds were coded as binary traits (presence/absence) for each species. As long as at least one individual of a species contained a given PA, we coded the occurrence of this PA as present, as it indicated that the species has the potential to produce this PA. The evolutionary history of each compound was traced across the ML topology of the total plastid and nuclear evidence using ML methods as implemented in Mesquite 3.6 (https://www.mesquiteproject.org/).

Besides the qualitative aspects of PA composition, we also applied phylogenetic studies to quantitative PA data. We used statistics K (Blomberg et al., 2003) and λ (Pagel, 1999) to estimate the strength of phylogenetic signals of continuous PA traits (absolute and relative concentrations) for each species. Values of K or λ indicate whether the distribution of a trait is phylogenetically random (K or $\lambda \approx 0$) or non-random (K or $\lambda \approx 1$). The significance (P) of each K estimate was assessed by randomization test with 10 000 trait simulations. The significance (P) of each λ was evaluated with a likelihood ratio test, where the likelihood of observed λ estimated from the tree was compared with the likelihood of $\lambda = 1$. The tests were conducted using the "phylosig" function in the "phytools" package. P-values were adjusted for multiple comparisons by sequential Bonferroni methods using the "p.adjust" function in the "stats" package. All analyses were conducted in R version 3.5.1.

3 Results

3.1 Pyrrolizidine alkaloid diversity of *Jacobaea* species
We analyzed 80 PAs with LC–MS/MS extracted from the leaves of 17 *Jacobaea* species encompassing multiple populations and individuals grown in a climate chamber. The 80 PAs were classified into five structural groups, that is, senecionine-like, erucifoline-like, jacobine-like, platyphylline-like, otosenine-like (Fig. 1), and unknown PAs (Additional file S1). Besides otosenine-like PAs that do not occur as *N*-oxides, the other five groups contain both tertiary (free base) and *N*-oxide forms.

The mean concentrations of total PAs, the sum free bases and *N*-oxides, and the sum PA structural groups between different species and different populations were compared (Table 1). The average total PA concentrations in different populations ranged from 6.2 (*J. cannabifolia* 1) to 4301.3 (*J. vulgaris* 2) μg/g dry weight (DW). Even within species, considerable variations of mean total PA concentrations were observed between accessions for some species, such as *J. carniolia* and *J. alpina*. In general, *J. vulgaris s.l.* group contained more accessions with high amounts of PAs. Pyrrolizidine alkaloid free bases were predominant in *J. abrotanifolia*, *J. vulgaris*, *J. maritima*, and *J. cannabifolia*, whereas PA *N*-oxides were dominant in *J. incana* and *J. subalpina*. However, a lack of consistency in the ratios of free bases and *N*-oxides seemed common between different accessions within *Jacobaea* species. Taking *J. aquatica* as an example, in the first accession, free bases took up to 78.8%, whereas in the second accession, free bases only accounted for 17.9%. Different chemotypes were found for some species including *J. adonidifolia* (erucifoline-type and otosenine-type), *J. aquatica* (senecionine-type and otosenine-type), *J. cannabifolia* (jacobine-type and mixed-type), and *J. paludosa* (jacobine-type and otosenine-type).

To compare differences of PA profiles among and within the *Jacobaea* species more comprehensively, we performed PCA using absolute concentrations, relative concentrations, and the presence/absence of PA traits of each *Jacobaea* plant. The distribution patterns based on these three aspects of PA traits were highly similar, with only slight changes of distances (or dispersion) between observations (Figs. 2A, S1A, S1C). Most of the *Incani* s.l. group was separated from the *J. vulgaris* s.l. group based on PC1 and PC2 (Figs. 2A, S1A, S1C). The classification resulted mainly from the differences in senecionine-like, jacobine-like, and otosenine-like PAs (Figs. 2B, S1B, S1D). The *Incani* s.l. group had higher contents of either particular senecionine-like or otosenine-like PAs, whereas the *J. vulgaris* s.l. group was characterized by more senecionine-like or jacobine-like PAs. Meanwhile, a high degree of overlap between the *J. paludosa* group and both of the other two groups is shown in PCA (Figs. 2A, S1A, S1C), clustering mainly below the axis along PC2. This distribution was caused by the lower amount or absence of some senecionine-like PAs (Figs. 2B, S1B, S1D) in the *J. paludosa* group. At the species level, plants were mainly clustered in species-specific ways, except that *J. subalpina* and *J. arnautorum* could not be distinguished from each other based on five principal components (Figs. S2–S4). The PA
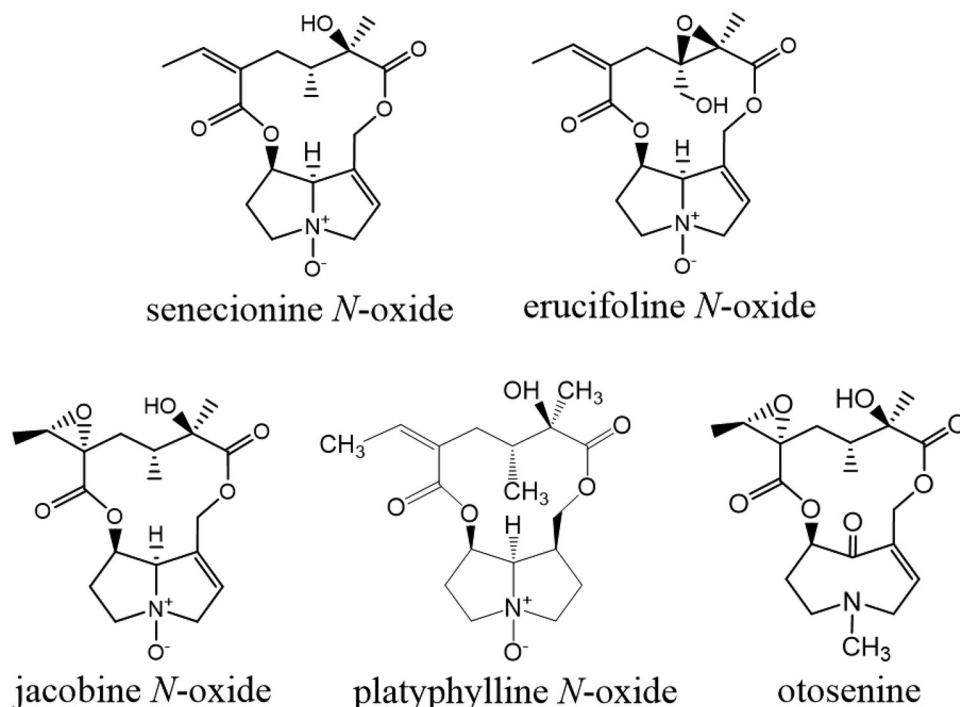
Fig. 1. Structural formulas representative of the five different structural groups of pyrrolizidine alkaloids (PAs).

patterns of different populations within some species were different, such as the cases of *J. aquatica* and *J. paludosa* (Figs. 2A, S1A, S1C).

We also performed HCA, giving information on closeness between *Jacobaea* plants based on the similarities of their PA bouquets. The clustering results based on the abovementioned three aspects of PA traits of all *Jacobaea* plants are shown as heatmaps (Figs. 3, S5, S6). To a large extent, in all cases, the plants appeared to be clustered in species-specific ways; however, some exceptions were found. Some species were grouped together, like the cluster of *J. subalpina* and *J. arnautorum*, and the cluster of *J. incana*, *J. leucophylla*, and *J. uniflora*. Some species showed species-specific PA patterns, but intraspecies variation surpassed interspecies differences. For example, the plants of *J. paludosa*, *J. alpina*, and *J. aquatica* were always clustered into two different subclusters within the species in population-specific ways (Figs. 3, S5, S6). Both *J. adonidifolia* and *J. cannabifolia* had two subclusters based on absolute concentrations or the presence/absence of PAs, but they had only one cluster based on relative concentrations. *J. maritima* had two subclusters based on the presence/absence of PA traits, but only one cluster when using either absolute or relative concentrations. Besides the clustering differences within species, the distances based on PA datasets among species varied using different aspects of PA traits. In all cases, the species could be divided into four sets loosely, based on their closeness of PA profiles, without considering their relative positions within each set (Figs. 3, S5, S6): *J. vulgaris*-related set (*J. vulgaris*, *J. maritima*, *J. paludosa*, *J. gnaphalioides*, *J. analoga*), *J. aquatica*-related set (*J.*

aquatica, *J. erucifolia*, *J. alpina*), *J. subapina*-related set (*J. subalpina*, *J. arnautorum*, *J. carniolia*, *J. incana*, *J. uniflora*, *J. leucophylla*), and *J. abrotanifolia*-related set (*J. abrotanifolia*, *J. adonidifolia*, *J. paludosa*). Nevertheless, the *J. vulgaris*-related set was more closely related to the *J. aquatica*-related set by absolute concentrations or present/absent PAs than by relative concentrations. Also, *J. cannabifolia* shifted its position from the *J. vulgaris*-related set to the *J. abrotanifolia*-related cluster when relative concentrations or binary PA traits were replaced by absolute concentrations.

Moreover, we evaluated covariations between individual PAs by Spearman's rank correlations based on PA information extracted from all *Jacobaea* plants. On the basis of absolute concentrations, 80 PAs were roughly clustered into four clusters (Fig. 4). The PAs within the derived structural groups (erucifoline-like, jacobine-like, platyphylline-like) were clustered together, even though there were some exceptions, whereas basic PAs (senecionine-like PAs) were distributed into different clusters. Erucifoline-like PAs and otonesine-like PAs were clustered in the same group (cluster 1). Jacobine-like PAs (cluster 3) and platyphylline-like PAs (cluster 4) were mainly assigned to separate clusters. Senecionine-like PAs had a scattered distribution across different clusters. Noticeably, otosenine-like PAs were negatively correlated to jacobine-like PAs, as well as to most of senecionine-like PAs. In general, the tertiary form of PAs had a high correlation with its corresponding *N*-oxide form. Similar patterns were found in HCAs of relative concentrations and presence/absence of PAs (Figs. S7, S8).
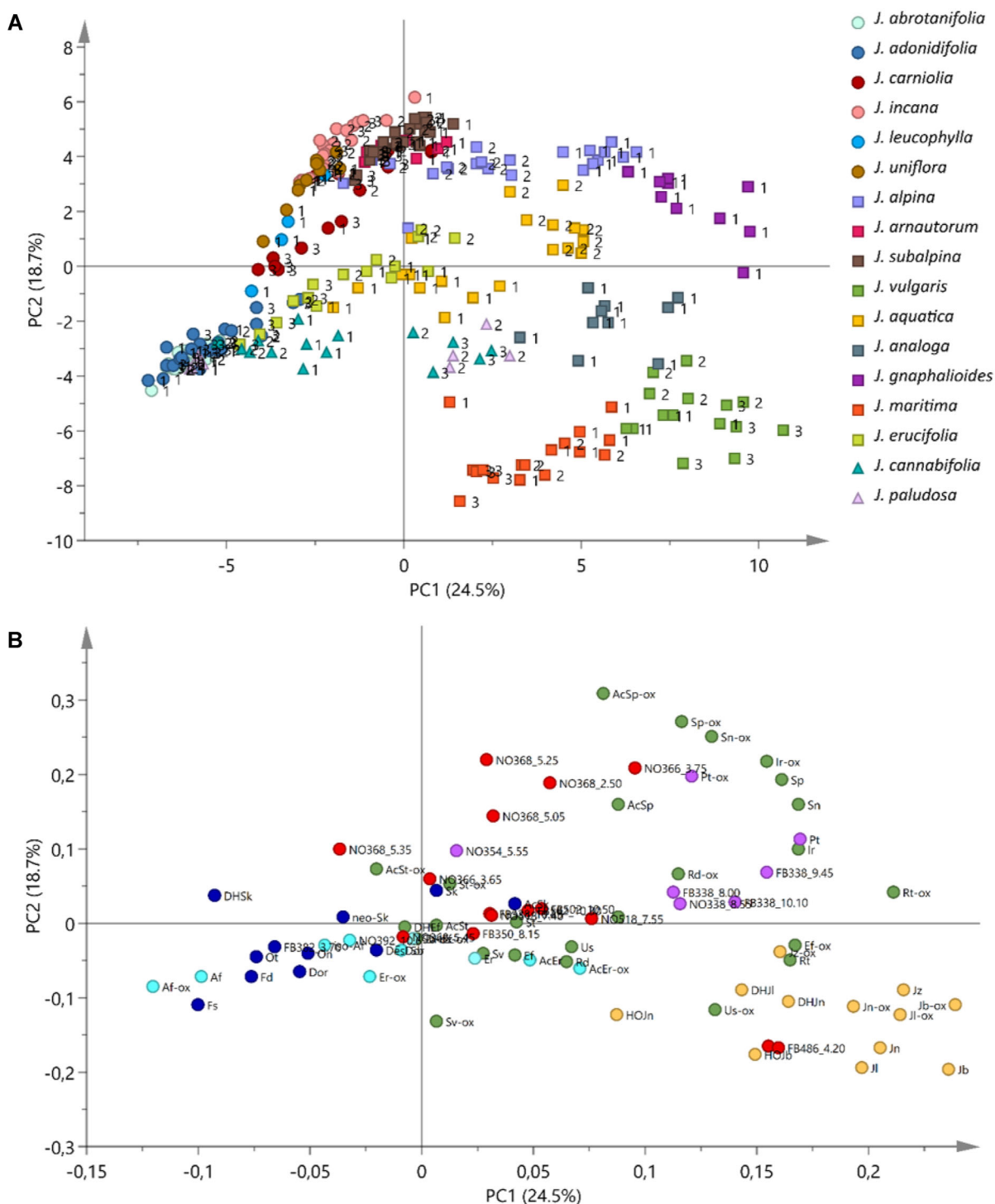
Fig. 2. Principal component analyses (PCA) based on absolute concentrations of 80 pyrrolizidine alkaloids (PAs) from multiple individuals and populations of 17 *Jacobaea* species grown in a climate chamber. **A,** The PCA score plot from SIMACA 15.0.2, based on the log-transformed and Pareto-scaled absolute concentrations of 80 PAs. PC1 and PC2 explain 24.5% and 18.7% of the variation, respectively. Each dot represents one plant individual. The number to the right of each dot represents different accessions (Table 1). Different species are coded by different colors, as indicated in the legend. Different phylogenetic groups are coded by different shapes: circle (*Incani* group), square (*J. vulgaris* group), triangle (*J. paludosa* group). **B,** The corresponding PCA loading plot. Each dot represents one PA. Abbreviations of PAs are listed in Additional file S1. Different structural groups of PAs are coded by different colors: green (senecionine-like), yellow (jacobine-like), light blue (erucifoline-like), dark blue (otosenine-like), purple (platyphylline-like), red (unknown).
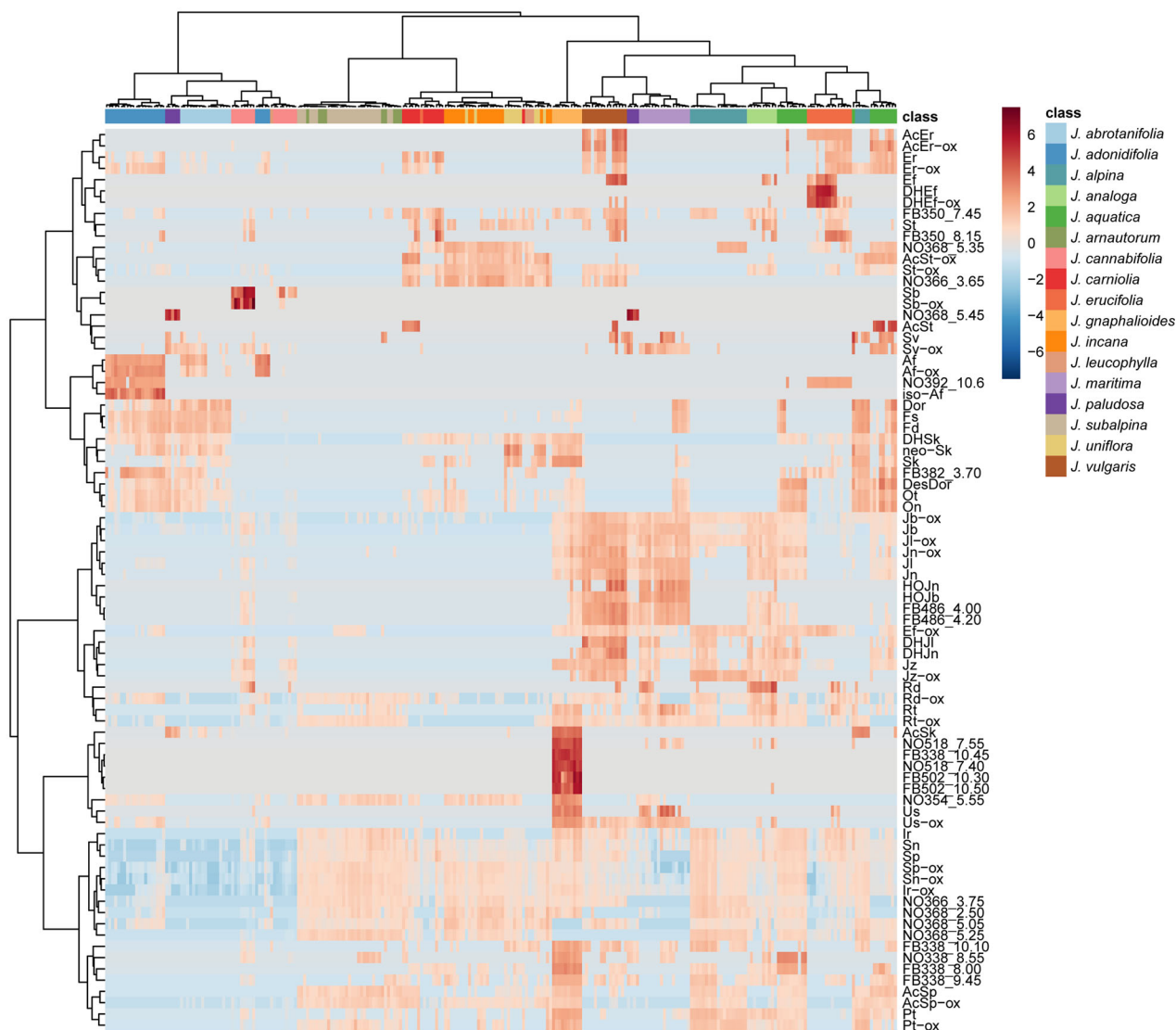
Fig. 3. Heatmap representing hierarchical clustering analysis of all individual *Jacobaea* plants based on the absolute concentrations of 80 pyrrolizidine alkaloids (PAs). The analysis was calculated with Euclidean distances and the Ward clustering algorithm based on the log-transformed and Pareto-scaled absolute concentrations of PAs in the tool MetaboAnalyst. The tree diagram at the top indicates the closeness between different *Jacobaea* plants with regard to PA composition and concentration. Different species are color-coded as indicated in the right-most legend. PA name abbreviations are shown in Additional file S1.

3.2 Phylogeny of *Jacobaea* species

To obtain "roadmaps" for tracing the evolutionary origin of PA diversity, we included 17 *Jacobaea* species to reconstruct the phylogeny with *S. vulgaris* as the outgroup in this study. In total, 11 plastid and three nuclear DNA makers were amplified and sequenced (Table S1), which were all included in phylogenetic trees ending up to a total length of 7590 bp. We used different statistical methods (ML, BI, MP) to recover historical relationships based on the combined plastid and nuclear dataset. The topologies of phylogenetic trees obtained by ML and BI were nearly identical, and were thus represented by the same cladogram, where high BS values coincided with high PP (Fig. 5). The consensus cladogram was largely in agreement with the phylogenetic

cladogram based on DNA sequences and morphological dataset in the previous study (Pelser et al., 2004). The three main clades found earlier were strongly supported: *Incani* s.l. group (*J. abrotanifolia*, *J. adonidifolia*, *J. carniolia*, *J.uniflora*, and *J. leucophylla*), *J. vulgaris* s.l. group (*J. alpina*, *J. subalpina*, *J. vulgaris*, *J. analoga*, *J. maritima*, *J. aquatica*, *J. arnautorum*, *J. gnaphalioides*, and *J. erucifolia*), and *J. paludosa* group (*J. cannabifolia* and *J. paludosa*). The *Incani* s.l. group was the most basal clade of *Jacobaea* species as a monophyletic clade in ML and BI phylogeny. For the *J. vulgaris* s.l. group, the phylogenetic relationships of seven closely related species (*J. alpina*, *J. analoga*, *J. aquatica*, *J. arnautorum*, *J. maritima*, *J. subalpina*, and *J. vulgaris*) still could not be resolved completely using the ML and BI algorithms based on the
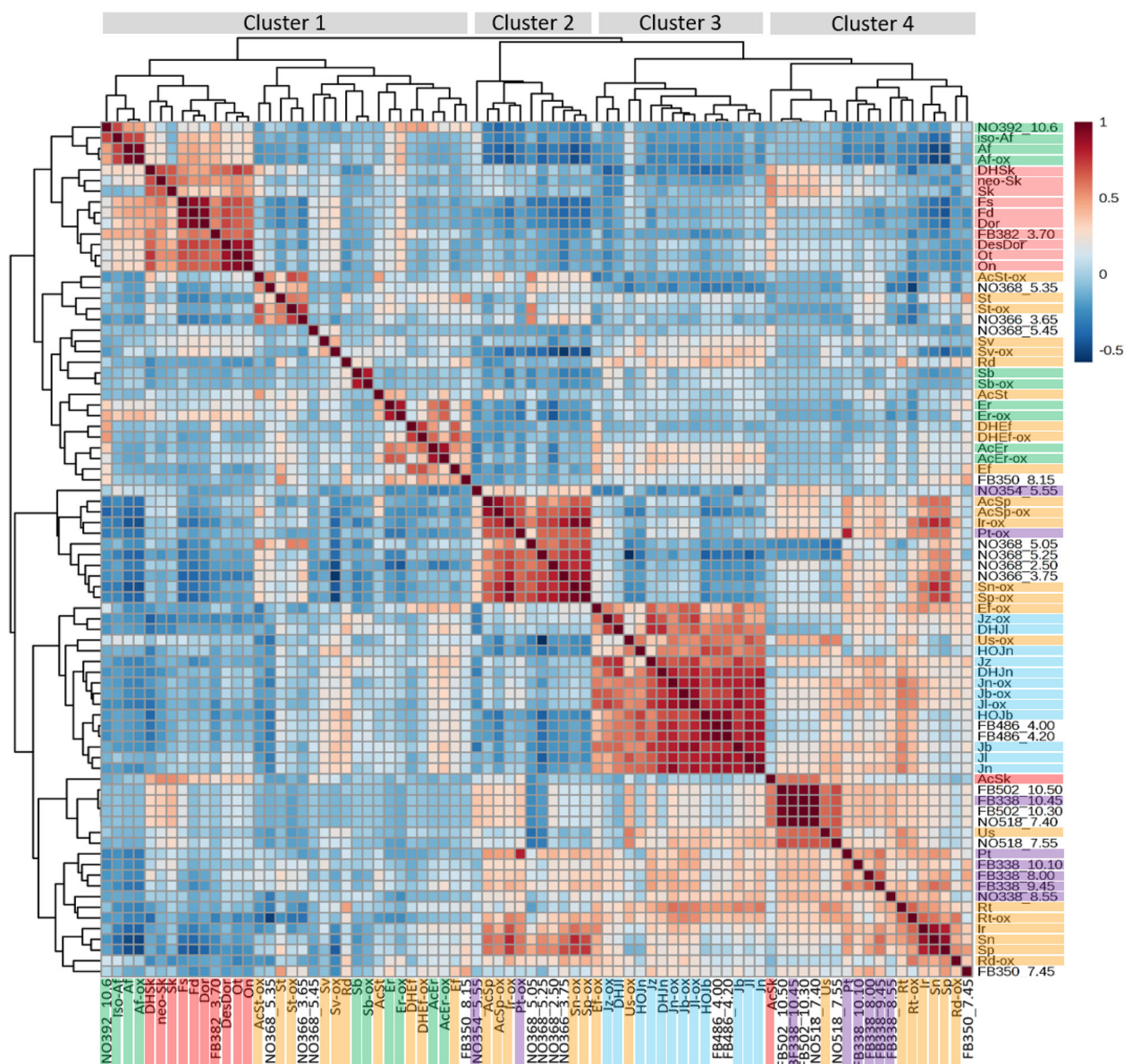
Fig. 4. Heatmap representing Spearman's rank correlation coefficients between individual pyrrolizidine alkaloids (PAs) based on absolute concentrations of PAs of all *Jacobaea* species. The analysis was calculated with Euclidean distances and the Ward clustering algorithm based on the log-transformed and Pareto-scaled absolute concentrations of PAs in the tool MetaboAnalyst. Positive correlations are displayed in red and negative correlations in blue, as indicated by the color scale on the right. Names of different known PA structural groups are highlighted with different colors: senecionine-like PAs (orange), erucifoline-like PAs (green), jacobine-like PAs (blue), platyphylline-like PAs (purple), otonesine-like PAs (red). PA name abbreviations are shown in Additional file S1.

DNA regions studied. By using the MP algorithm, it was observed that the *Incani* s.l. group was a polyphyletic assemblage (Fig. S9). A better resolution of phylogenetic relationship was obtained for the *J. vulgaris* s.l. group. All BS values were over 70%, except for the placement of *J. analoga* to the clade composed of *J. alpina*, *J. subalpina*, and *J. vulgaris*. The clade of *J. aquatica* and *J. arnautorum* was more closely related to *J. gnaphalioides* than the other five species aforementioned. As the ML algorithm determined the best-fit substitution model and showed exactly the same result as the BI algorithm, we used the ML phylogenetic tree in the

following steps for ancestral state reconstruction and the check of phylogenetic signals.

3.3 Ancestral state reconstruction and phylogenetic signals
We traced the evolutionary history of PA formation (presence/absence) using the ML phylogeny (Fig. S10) based on the total plastid and nuclear evidence as the "roadmap." Of the 80 PAs detected by LC–MS/MS, six (senecionine, senecionine *N*-oxide, integerrimine *N*-oxide, seneciphylline, seneciphylline *N*-oxide, and riddelliine *N*-oxide) were present in all species, whereas eight
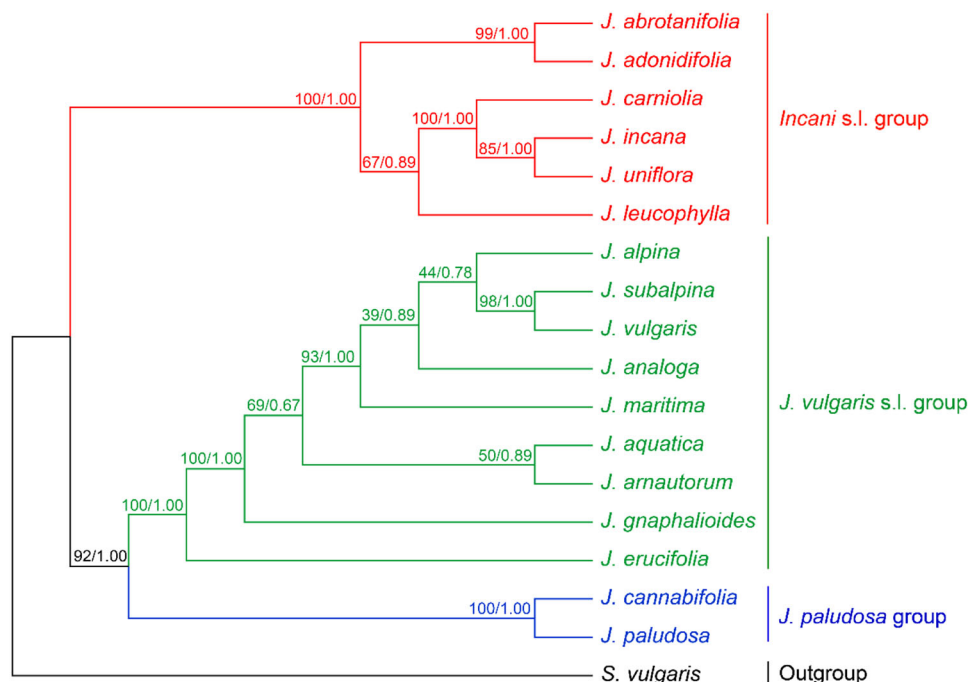
Fig. 5. Maximum likelihood (ML) and Bayesian inference (BI) consensus cladogram of 17 *Jacobaea* species inferred from the combined plastid and nuclear dataset. ML bootstrap values and Bayesian posterior probabilities (BS/PP) are indicated above the branches. Different groups are color-coded: *Incani* s.l. group (red), *J. vulgaris* s.l. group (green), *J. paludosa* group (blue), and outgroup *S. vulgaris* (black).

(dehydroeruciflorine, senecicannabine, senecicannabine *N*-oxide, iso-adonifoline, and the unidentified PAs FB338 [10.45], NO386 [5.45], FB502 [10.30], and NO518 [7.40]) were unique to a single species. Evolutionary patterns of the remaining PAs were complex, showing irregular presences or absences of individual PAs. Quite often, PAs showed frequent "on/off" changes without noticeable evolutionary direction (Additional file S2). This was well illustrated by the evidence that all three clades of *Jacobaea* species contain both species with or without certain PAs such as erucifoline *N*-oxide (Fig. 6A). On the contrary, some PAs seemed to have originated or been lost only a few times in parallel. Examples of this pattern included the absence of senkirkine (Fig. 6B) and the presence of adonifoline (Fig. 6C). Unlike the patterns mentioned previously, jaconine *N*-oxide was the only PA identified in our study, whose occurrence showed a clear evolutionary direction, as this PA was absent in all species of the *Incani* s.l. clade and present in all species of the other two clades (*J. vulgaris* s.l. clade and *J. paludosa* clade; Fig. 6D).

A phylogenetic signal is defined as the tendency of related species to resemble each other more than they resemble species drawn at random from the tree (Blomberg & Garland, 2002). We used two quantitative measures, namely Blomberg et al.'s (2003) K and Pagel's (1999) λ, to measure phylogenetic signals of continuous PA traits (average absolute and relative concentrations) for each species. After sequential Bonferroni adjustment, only three PAs (i.e., dehydroeruciflorine, dehydroeruciflorine *N*-oxide, and NO368 [5.45]) showed significant phylogenetic signals ($\lambda \approx 1$; $P < 0.05$) under λ statistics in their absolute concentrations (Additional file S3). Of these three PAs, dehydroeruciflorine was unique to *J. erucifolia*, whereas NO368 [5.45] was unique to *J. paludosa*. Dehydroeruciflorine *N*-oxide was detected in *J. erucifolia* as well as in *J. vulgaris* and *J. analoga* with low amounts only in a few individuals of the latter two species. For relative concentrations, under λ statistics, nine PAs (integerrimine, senecivernine *N*-oxide, eruciflorine, eruciflorine *N*-oxide, dehydroeruciflorine, dehydroeruciflorine *N*-oxide, erucifoline *N*-oxide, acetylerucifoline, and NO368 [5.45]) showed significant phylogenetic signals. None of the PAs showed significant phylogenetic signals by K statistics, either in absolute or relative concentrations (Additional file S3).

4 Discussion

We observed flexible PA profiles among 17 different *Jacobaea* species with respect to both quantitative and qualitative PA variations, showing both high inter-/intraspecies PA diversity, which supports previous findings (Hartmann & Dierich, 1998; Macel et al., 2004; Pelser et al., 2005; Langel et al., 2011). In total, 80 PAs were detected, including both free bases and *N*-oxides in this study, which covered all 26 PAs reduced to the tertiary form, except sennecicannabine and deacetyldoronine detected in the study of Pelser et al. (2005). In our study, the average total PA concentration of a species ranged from 32.9 (*J. cannabifolia*) to 3835.7 (*J. gnaphalioides*) μg/g DW. More accessions in *J. vulgaris* s.l. group contained higher total PA concentrations (Table 1). To the best of authors' knowledge, there is no relationship between the total PA amount and the
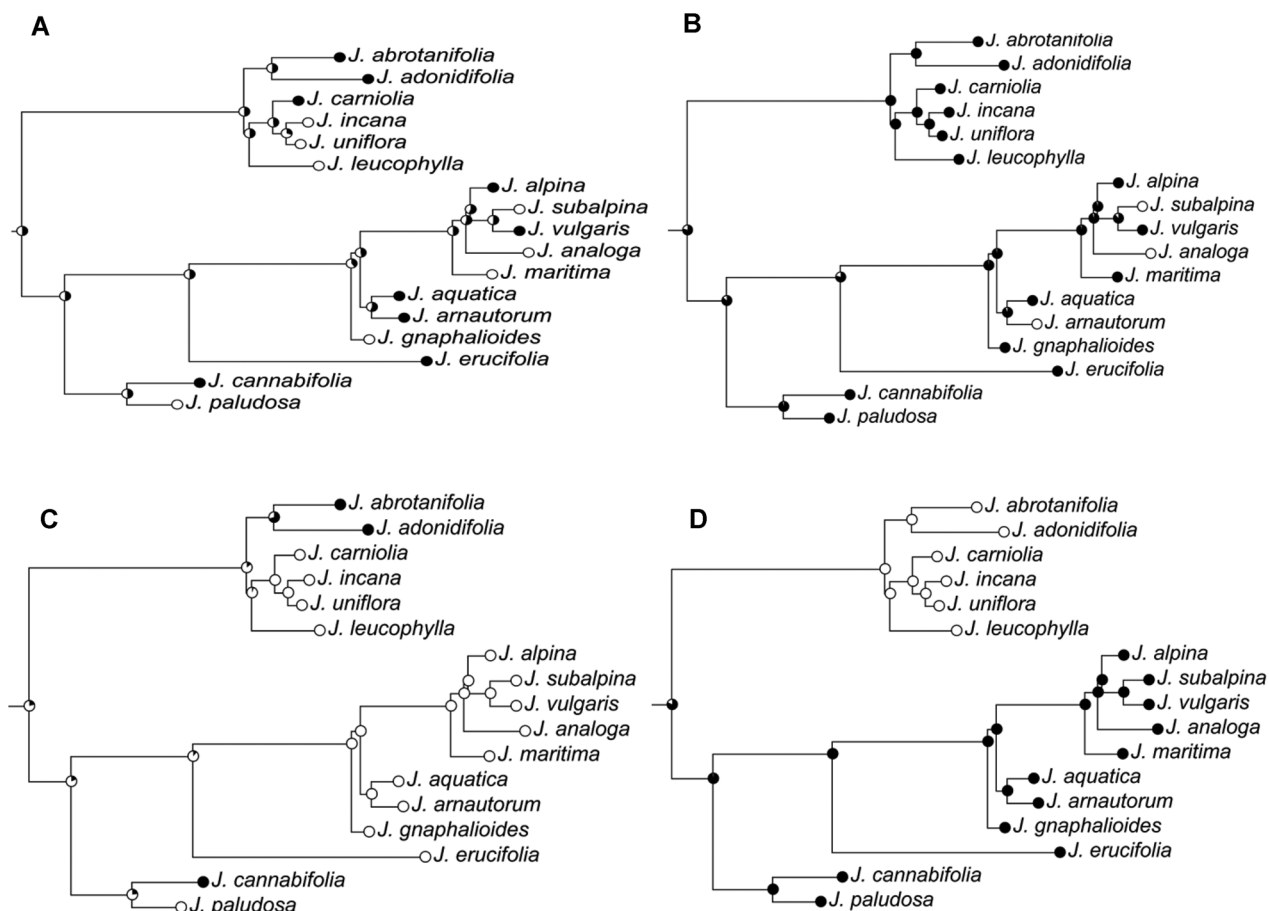
Fig. 6. Maximum likelihood ancestral state reconstruction of four pyrrolizidine alkaloids (PAs). The tree shown is the maximum likelihood (ML) tree from the total plastid and nuclear dataset of 17 *Jacobaea* species. **A,** erucifoline *N*-oxide. **B,** senkirkine. **C,** adonifoline. **D,** jaconine *N*-oxide. Character states were binary-coded for each species and are shown as small pie charts before taxon names: black (presence) and white (absence). The pie charts shown at individual nodes illustrate the likelihood for the ancestral states.

genome size or chromosome number (data not shown). The numbers of PAs varied from 21 (*J. leucophylla*) to 59 (*J. aquatica*), with different relative abundances between different species. Both PA concentrations and compositions were confirmed to be species-specific; however, in some cases, PA patterns from different populations within species differed from each other and even surpassed differences between species (Figs. 2, 3, S1–S6). However, the taxonomic relationships derived from qualitative and quantitative PA profiles of different *Jacobaea* species are inconsistent with their phylogenetic relationships based on molecular markers. For instance, *J. abrotanifolia* and *J. adonidifolia* were always grouped with the other four species of the *Incani* s.l. clade in different clusters based on their PA patterns (Figs. 3, S5, S6), which is incongruent with the *Incani* s.l. cluster on phylogenetic trees (Figs. 5, S9, S10). On a closer look, we examined the occurrences and phylogenetic signals of individual PAs using the mean phylogeny of 17 *Jacobaea* species as the "roadmap." By tracing the evolutionary history of PA formation (presence/absence), we found that except the PAs unique to a single species or ubiquitous among all species, PAs appear to be distributed incidentally within the genus *Jacobaea*, revealing

limited phylogenetic signals, which is in agreement with the findings of Pelser et al. (2005). For quantitative PA data, none of the PAs showed significant phylogenetic signals under *K* statistics, whereas nine of the 80 PAs showed phylogenetic signals based on relative and/or absolute concentrations under λ statistics. These results were similar to those indicated for terpenoids in Lamiaceae, as only 25% (14 out of 57 without a multiple-comparison correction) of the tested monoterpenes showed significant phylogenetic signals for their presence/absence at the species level (Mint Evolutionary Genomics Consortium, 2018). We also performed PCAs, HCAs, and ancestral state reconstruction using each structural type of PAs as a unit, showing no better classification of *Jacobaea* species (Figs. S11, S12) and no stronger phylogenetic signals (Fig. S13) as compared with the results based on individual PAs. This evidence suggests that the distributions of different individual SMs or structural groups within a chemical class on phylogenetic trees are often random, lacking phylogenetic signals.

Chemical diversity is attributable to the effects of genetic variation, environmental influences, and the interaction between these two factors (Moore et al., 2014; Kessler &

Kalske, 2018). In our study, we grew all the plants under the same condition, aiming at minimizing environmental variation. It was demonstrated that the individual PA bouquets were brought about by genetically controlled specific processes in *Senecio* and *Jacobaea* species (Hartmann & Dierich, 1998). Under controlled conditions, 50%–100% of the total variation in total PA concentration of *J. vulgaris* was due to genetic differences (Vrieling et al., 1993), and PA composition and concentration were genotype-dependent (Macel et al., 2004; Cheng et al., 2011). However, the phylogenetic distances of *Jacobaea* species were not correlated with differences in their PA bouquets. Even within species, different populations that had highly similar DNA sequences showed rather different PA patterns, such as the case of the two populations of *J. paludosa*. This discrepancy between PA profiles and phylogenetic relationships might be due to their maternal effects or gene–environment interactions. According to Kessler & Kalske (2018), organisms interacting with plants can use SM bouquets to find appropriate hosts. With varying SM profiles, plants should lower the chance of attack from herbivores by diverting chemical compositions away from a common host search pattern used by a potential herbivores. If this process would be stronger within phylogenetically related plants, it would decrease the phylogenetic signals of the SMs. Compared with traits such as morphological characters, SMs may be under weak evolutionary constraints due to relatively lower production costs. As long as evolutionary constraints are not limiting the response to selection, even relatively weak selection can lead to adaptive changes, thus resulting in the losses and gains of SMs (Kessler & Kalske, 2018). This rapid evolutionary fine-tuning might be excellent mechanistic basis for plants to cope with multiple selective forces.

The composition of plant SMs is vital in determining the evolutionary success of populations and species (Burow et al., 2010). Different SMs may have played different roles during plant evolution and have been exposed to different selective forces. Statistically, jacobine-like PAs, senecionine-like PAs, and otosenine-like PAs played more important roles in the classification of different *Jacobaea* species quantitatively and qualitatively in PCA (Figs. 2B, S1B, S1D), which suggests that these PAs may be involved in speciation. Senecionine-like PAs have been regarded as biosynthetically basic PAs and can be found in all *Jacobaea* species. The total amount of PAs in plants is controlled by the formation of senecionine *N*-oxide in roots, and the constitutive biosynthesis of senecionine *N*-oxide is genotype-dependent (Hartmann & Dierich, 1998). Jacobine-like PAs have a higher percentage of free bases and otosenine-like PAs are only present as free bases, which are regarded as biosynthetically more derived PAs. In general, free base PAs resulted in a lower survival of insect herbivores as compared with *N*-oxides (Liu et al., 2017). Cheng et al. (2013) found that tertiary amines of jacobine-like PAs and some otosenine-PAs were positively correlated with the oviposition preferences of the specialist herbivore cinnabar moth. Interestingly, most erucifoline-like PAs only had marginal weights in the classification of different species in PCA. Wei et al. (2019) used methyl jasmonate to treat *J. vulgaris* and *J. aquatica* mimicking the effects of herbivory, and they found a strong shift from senecionine-like PAs to erucifoline-like PAs in both

species. This might reveal that *Jacobaea* species have a similar defense strategy related to erucifoline-like PAs.

Although previous tracer feeding experiments showed senecionine *N*-oxide as the backbone structure of most PAs in *Senecio* (Hartmann & Toppel, 1987; Toppel et al., 1987; Hartmann & Dierich, 1998), the exact sequences and biosynthetic reactions of PA conversions remain unclear. The HCAs of individual PAs (Figs. 4, S7, S8) in our study showed that individual PAs within the same structural groups of more biosynthetically derived PAs (jacobine-like, erucifoline-like, platyphylline-like, and otosenine-like) had higher correlations for their expression as compared with those of senecionine-like PAs, which is largely in agreement with the findings of Cheng et al. (2011). The positive correlations of PAs within each structural group indicate that the diversification within each group may be passive and codependent processes. The negative correlations between different structural groups revealed possible active and competitive processes of transformations. Nonetheless, jacobine-like PAs showed positive correlations with most of platyphylline-like PAs, revealing a codependent expression of these two structural groups in the PA biosynthetic pathway.

Two assumptions were made on the gene level to explain why individual PAs irregularly appear and disappear on the phylogenetic tree: (i) PA-specific genes have evolved several times among *Jacobaea* species; (ii) all *Jacobaea* species possess the machinery to produce all PAs, but some PA specific genes are not expressed in some species. Given the prevalent intraspecific PA diversity, and the detection of "unique" PAs in more species in other studies, for example, dehydroerucifolorine was detected in *J. vulgaris* by Carvalho et al. (2014), we speculate that the latter assumption is most likely, even though the modes of action involved in biosynthetic pathways of PAs are unclear. To test this hypothesis, we need to understand the molecular basis of PA biosynthesis.

In conclusion, we analyzed PA profiles of 17 *Jacobaea* species including multiple individuals and populations, quantitatively and qualitatively. Both PA concentrations and compositions were confirmed to be species-/population-specific. The PAs driving the classification may implicate their important roles in ecological processes of different species. By tracing the occurrence and evaluating the phylogenetic signal of each PA trait, we found that PAs were more incidentally distributed along the phylogeny with limited phylogenetic signals. We, therefore, speculate that the PA diversity among and within *Jacobaea* species is more likely the result of differential expressions of PA biosynthesis genes as a life strategy in response to different biological needs, rather than the result of gains and losses of particular PA biosynthesis genes during evolution.

Acknowledgements

Jardins botaniques du Grand Nancy et de l'Université de Lorraine, Palace and Botanical Gardens of Balchik, Polish Academy of Sciences Botanical Garden Center for Biological Diversity Conservation in Powsin and Royal Botanic Gardens Kew for donating seeds. They also thank Karin van der Veen-van Wijk, Maria Franco Berriel, and Rick Hennevelt for their technical assistance, Dr. Young Hae Choi for his kind support for the SIMCA software, and Martine Huberty for her discussion about statistical analyses.

References

Abadi S, Azouri D, Pupko T, Mayrose I. 2019. Model selection may not be a mandatory step for phylogeny reconstruction. *Nature Communications* 10: 934.

Altekar G, Dwarkadas S, Huelsenbeck JP, Ronquist F. 2004. Parallel Metropolis-coupled Markov chain Monte Carlo for Bayesian phylogenetic inference. *Bioinformatics* 20: 407–415.

Blomberg SP, Garland T Jr. 2002. Tempo and mode in evolution: Phylogenetic inertia, adaptation and comparative methods. *Journal of Evolutionary Biology* 15: 899–910.

Blomberg SP, Garland T, Ives AR. 2003. Testing for phylogenetic signal in comparative data: Behavioral traits are more labile. *Evolution* 57: 717–745.

Burow M, Halkier BA, Kliebenstein DJ. 2010. Regulatory networks of glucosinolates shape *Arabidopsis thaliana* fitness. *Current Opinion in Plant Biology* 13: 348–353.

Carvalho S, Macel M, Mulder PPJ, Skidmore A, van der Putten WH. 2014. Chemical variation in *Jacobaea vulgaris* is influenced by the interaction of season and vegetation successional stage. *Phytochemistry* 99: 86–94.

Castells E, Mulder PPJ, Pérez-Trujillo M. 2014. Diversity of pyrrolizidine alkaloids in native and invasive *Senecio pterophorus* (Asteraceae): Implications for toxicity. *Phytochemistry* 108: 137–146.

Cheng D, Hirk H, Mulder PPJ, Vrieling K, Klinkhamer PGL. 2011. Pyrrolizidine alkaloid variation in shoots and roots of segregating hybrids between *Jacobaea vulgaris* and *Jacobaea aquatica*. *New Phytologist* 192: 1010–1023.

Cheng D, van der Meijden E, Mulder PPJ, Vrieling K, Klinkhamer PGL. 2013. Pyrrolizidine alkaloid composition influences cinnabar moth oviposition preferences in *Jacobaea* hybrids. *Journal of Chemical Ecology* 39: 430–437.

Chong J, Soufan O, Li C, Caraus I, Li S, Bourque G, Wishart DS, Xia J. 2018. MetaboAnalyst 4.0: Towards more transparent and integrative metabolomics analysis. *Nucleic Acids Research* 46: W486–W494.

Chou MW, Fu PP. 2006. Formation of DHP-derived DNA adducts *in vivo* from dietary supplements and Chinese herbal plant extracts containing carcinogenic pyrrolizidine alkaloids. *National Center for Toxicological Research* 22: 321–327.

Courtois EA, Dexter KG, Paine CET, Stien D, Engel J, Baraloto C, Chave J. 2015. Evolutionary patterns of volatile terpene emissions across 202 tropical tree species. *Ecology and Evolution* 6: 2854–2864.

Hartmann T. 1996. Diversity and variability of plant secondary metabolism: a mechanistic view. *Entomologia Experimentalis et Applicata* 80: 177–188.

Hartmann T. 1999. Chemical ecology of pyrrolizidine alkaloids. *Planta* 207: 483–495.

Hartmann T, Dierich B. 1998. Chemical diversity and variation of pyrrolizidine alkaloids of the senecionine type: biological need or coincidence? *Planta* 206: 443–451.

Hartmann T, Ehmke A, Eilert U, von Borstel K, Theuring C. 1989. Site of synthesis, translocation and accumulation of pyrrolizidine alkaloid N-oxides in *Senecio vulgaris* L. *Planta* 177: 98–107.

Hartmann T, Toppel G. 1987. Senecionine N-oxide, the primary product of pyrrolizidine alkaloid biosynthesis in root cultures of *Senecio vulgaris*. *Phytochemistry* 26: 1639–1643.

Joosten L, Mulder PPJ, Vrieling K, van Veen JA, Klinkhamer PGL. 2010. The analysis of pyrrolizidine alkaloids in *Jacobaea vulgaris*; a comparison of extraction and detection methods. *Phytochemical Analysis* 21: 197–204.

Kalyaanamoorthy S, Minh BQ, Wong TKF, von Haeseler A, Jermiin LS. 2017. ModelFinder: Fast model selection for accurate phylogenetic estimates. *Nature Methods* 14: 587–589.

Kessler A, Kalske A. 2018. Plant secondary metabolite diversity and species interactions. *Annual Review Ecology, Evolution, and Systematics* 49: 115–138.

Kliebenstein DJ, Kroymann J, Brown P, Figuth A, Pedersen D, Gershenzon J, Mitchell-Olds T. 2001. Genetic control of natural variation in *Arabidopsis* glucosinolate accumulation. *Plant Physiology* 126: 811–825.

Kumar S, Stecher G, Tamura K. 2016. MEGA7: Molecular evolutionary genetics analysis version 7.0 for bigger datasets. *Molecular Biology and Evolution* 33: 1870–1874.

Langel D, Ober D, Pelser PB. 2011. The evolution of pyrrolizidine alkaloid biosynthesis and diversity in the Senecioneae. *Phytochemistry Reviews* 10: 3–74.

Lewis PO. 2001. A likelihood approach to estimating phylogeny from discrete morphological character data. *Systematic Biology* 50: 913–925.

Liu X, Klinkhamer PGL, Vrieling K. 2017. The effect of structurally related metabolites on insect herbivores: A case study on pyrrolizidine alkaloids and western flower thrips. *Phytochemistry* 138: 93–103.

Macel M, Vrieling K, Klinkhamer PGL. 2004. Variation in pyrrolizidine alkaloid patterns of *Senecio jacobaea*. *Phytochemistry* 65: 865–873.

Maldonado C, Barnes CJ, Cornett C, Holmfred E, Hansen SH, Persson C, Antonelli A, Rønsted N. 2017. Phylogeny predicts the quantity of antimalarial alkaloids within the iconic yellow cinchona bark (Rubiaceae: *Cinchona calisaya*). *Frontiers in Plant Science* 8: 391.

Mint Evolutionary Genomics Consortium. 2018. Phylogenomic mining of the mints reveals multiple mechanisms contributing to the evolution of chemical diversity in Lamiaceae. *Molecular Plant* 11: 1084–1096.

Moore BD, Andrew RL, Külheim C, Foley WJ. 2014. Explaining intraspecific diversity in plant secondary metabolites in an ecological context. *New Phytologist* 201: 733–750.

Mulder PPJ, López P, Castelari M, Bodi D, Ronczka S, Preiss-Weigert A, These A. 2018. Occurrence of pyrrolizidine alkaloids in animal- and plant-derived food: Results of a survey across Europe. *Food Additives & Contaminants: Part A* 35: 118–133.

Nguyen LT, Schmidt HA, von Haeseler A, Minh BQ. 2015. IQ-TREE: A fast and effective stochastic algorithm for estimating maximum likelihood phylogenies. *Molecular Biology and Evolution* 32: 268–274.

Pagel M. 1999. Inferring the historical patterns of biological evolution. *Nature* 401: 877–884.

Pelser PB, van den Hof K, Gravendeel B, van der Meijden R. 2004. The systematic value of morphological characters in Senecio

Sect. Jacobaea (Asteraceae) as compared to DNA sequences. *Systematic Botany* 29: 790–805.

Pelser PB, de Vos H, Theuring C, Beuerle T, Vrieling K, Hartmann T. 2005. Frequent gain and loss of pyrrolizidine alkaloids in the evolution of *Senecio* section *Jacobaea* (Asteraceae). *Phytochemistry* 66: 1285–1295.

Ronquist F, Huelsenbeck JP. 2003. MRBAYES 3: Bayesian phylogenetic inference under mixed models. *Bioinformatics* 19: 1572–1574.

Sander H, Hartmann T. 1989. Site of synthesis, metabolism and translocation of senecionine N-oxide in cultured roots of *Senecio erucifolius*. *Plant Cell, Tissue and Organ Culture* 18: 19–31.

Soldaat LL, Boutin JP, Derridj S. 1996. Species-specific composition of free amino acids on the leaf surface of four *Senecio* species. *Journal of Chemical Ecology* 22: 1–12.

These A, Bodi D, Ronczka S, Lahrssen-Wiederholt M, Preiss-Weigert A. 2013. Structural screening by multiple reaction monitoring as a new approach for tandem mass spectrometry: Presented for the determination of pyrrolizidine alkaloids in plants. *Analytical Bioanalytical Chemistry* 405: 9375–9383.

Toppel G, Witte L, Riebesehl B, von Borstel K, Hartmann T. 1987. Alkaloid patterns and biosynthetic capacity of root cultures from some pyrrolizidine alkaloid producing *Senecio* species. *Plant Cell Reports* 6: 466–469.

Vaidya G, Lohman DJ, Meier R. 2011. SequenceMatrix: Concatenation software for the fast assembly of multi-gene datasets with character set and codon information. *Cladistics* 27: 171–180.

Vrieling K, de vos H, van wijk CAM. 1993. Genetic analysis of the concentration of pyrrolizidine alkaloids in *Senecio jacobaea*. *Phytochemistry* 32: 1141–1144.

Wei X, Vrieling K, Mulder PPJ, Klinkhamer PGL. 2019. Methyl jasmonate changes the composition and distribution rather than the concentration of defence compounds: A study on pyrrolizidine alkaloids. *Journal of Chemical Ecology* 45: 136–145.

Wiedenfeld H, Roeder E, Bourauel T, Edgar J. 2008. *Pyrrolizidine alkaloids: Structure and toxicity*. Bonn: V&R unipress GmbH.

Wink M. 2003. Evolution of secondary metabolites from an ecological and molecular phylogenetic perspective. *Phytochemistry* 64: 3–19.

Wink M. 2008. Plant secondary metabolism: Diversity, function and it evolution. *Natural Product Communications* 3: 1205–1216.

Witte L, Ernst L, Adam H, Hartmann T. 1992. Chemotypes of two pyrrolizidine alkaloid-containing *Senecio* species. *Phytochemistry* 31: 559–565.

Ziegler J, Facchini PJ. 2008. Alkaloid biosynthesis: Metabolism and trafficking. *Annual Review of Plant Biology* 59: 735–769.

Supplementary Material

The following supplementary material is available online for this article at http://onlinelibrary.wiley.com/doi/10.1111/jse.12671/suppinfo:

Fig. S1. PAs from different individuals and populations of 17 *Jacobaea* species grown in a climate chamber. (A) and (C): PCA score plots from SIMCA 15.0.2 based on the log-transformed and Pareto-scaled relative concentrations and Pareto-scaled presence/absence of 80 PAs, respectively. Each dot represents one plant individual. The number to the right of each dot represents different populations (Table1). Different species are coded by different colors as indicated in the legend. Different groups are coded by different shapes: circle (*Incani-group*), square (*J. vulgaris-group*), triangle (*J. paludosa-group*). (B) and (D): PCA loading plots responding to (A) and (C), respectively. Each dot represents one PA. Abbreviations of PAs are listed in Additional file S1. Different structural groups of PAs are coded by different colors: green (senecionine-like), yellow (jacobine-like), light blue (erucifoline-like), dark blue (otosenine-like), purple (platyphylline-like), red (unknown).

Fig. S2. PCA score plots of absolute PA concentration from different individuals and populations of 17 *Jacobaea* species grown in a climate chamber. The plots show the five auto-fit principal components based on the log-transformed and Pareto-scaled absolute concentrations of 80 PAs using the tool MetaboAnalyst. R^2 of each PC is shown in the figure. Each dot represents one plant individual. Different species are coded by different colors as indicated in the legend.

Fig. S3. PCA score plots of relative PA concentration from different individuals and populations of 17 *Jacobaea* species grown in a climate chamber. The plots show the five auto-fit principal components based on the log-transformed and Pareto-scaled relative concentrations of 80 PAs using the tool MetaboAnalyst. R^2 of each PC is shown in the figure. Each dot represents one plant individual. Different species are coded by different colors as indicated in the legend.

Fig. S4. PCA score plots of PAs from different individuals and populations of 17 *Jacobaea* species grown in a climate chamber. The plots show the five auto-fit principal components based on the Pareto-scaled presence/absence of 80 PAs using the tool MetaboAnalyst. R^2 of each PC is shown in the figure. Each dot represents one plant individual. Different species are coded by different colors as indicated in the legend.

Fig. S5. Heatmap representing hierarchical clustering analysis of all individual *Jacobaea* plants based on the relative concentrations of 80 PAs. The analysis was calculated with Euclidean distances and the Ward clustering algorithm based on the log-transformed and Pareto-scaled relative concentrations of PAs in the tool MetaboAnalyst. The tree diagram on the top indicates the closeness between different *Jacobaea* plants. Different species are color coded as indicated in the right-most legend. PA name abbreviations are shown in Additional file S1.

Fig. S6. Heatmap representing hierarchical clustering analysis of all individual *Jacobaea* plants based on the presence/absence of 80 PAs. The analysis was calculated with Euclidean distances and the Ward clustering algorithm based on Pareto-scaled presence (1)/absence (0) of PAs in the tool MetaboAnalyst. The tree diagram on the top indicates the closeness between different *Jacobaea* plants. Different species are color coded as indicated in the right-most legend. PA name abbreviations are shown in Additional file S1.

Fig. S7. Heatmap representing Spearman rank correlation coefficients between individual PAs based on relative concentrations of PAs of all individual *Jacobaea* plants. The analysis was calculated with Euclidean distances and the Ward clustering algorithm based on the log-transformed and Pareto-scaled relative concentrations of PAs in the tool MetaboAnalyst. Names of different known PA structural groups are highlighted with different colors: senecionine-like PAs (orange), erucifoline-like PAs (green), jacobine-like PAs (blue), platyphylline-like PAs (purple), otonesine-like PAs (red). PA name abbreviations are shown in Additional file S1.

Fig. S8. Heatmap representing Spearman rank correlation coefficients between individual PAs based on the presence/absence of PAs of all individual *Jacobaea* plants. The analysis was calculated with Euclidean distances and the Ward clustering algorithm based on Pareto-scaled presence (1)/absence (0) of PAs in the tool MetaboAnalyst. Names of different known PA structural groups are highlighted with different colors: senecionine-like PAs (orange), erucifoline-like PAs (green), jacobine-like PAs (blue), platyphylline-like PAs (purple), otonesine-like PAs (red). PA name abbreviations are shown in Additional file S1.

Fig. S9. Maximum parsimony (MP) strict consensus cladogram based on the combined plastid and nuclear data of 17 *Jacobaea* species. Bootstrap values are given at each node. Different groups are color coded: *Incani* s.l.-group (red), *J. vulgaris* s.l.-group (green), *J. paludosa*-group (blue), and outgroup *S. vulgaris* (black).

Fig. S10. Maximum likelihood (ML) phylogeny of 17 *Jacobaea* species inferred from the combined plastid and nuclear dataset. ML bootstrap values are indicated next to each node, and the scale bar is indicated in the top left corner. Different groups are color coded: *Incani* s.l.-group (red), *J. vulgaris* s.l.-group (green), *J. paludosa*-group (blue), and outgroup *S. vulgaris* (black).

Fig. S11. PCA score plots of PA structural groups from different individuals and populations of 17 *Jacobaea* species grown in a climate chamber. The plots show the five auto-fit principal components based on the log-transformed and Pareto-scaled sum of the individual PAs from each PA structural group (senecionine-, erucifoline-, jacobine-, platyphylline-, otosenine-like PAs and unknown PAs) using the tool MetaboAnalyst. (A) the sum of absolute concentrations; (B) the sum of relative concentrations. R^2 of each PC is shown in the figure. Each dot represents one plant individual. Different species are coded by different colors as indicated in the legend.

Fig. S12. Heatmap representing hierarchical clustering analysis of all individual *Jacobaea* plants based on the sum of individual PAs from each PA structural group (senecionine-, erucifoline-, jacobine-, platyphylline-, otosenine-like PAs and unknown PAs). The analyses were calculated with Euclidean distances and the Ward clustering algorithm based on the log-transformed and Pareto-scaled sum in the tool MetaboAnalyst: (A) the sum of absolute concentrations; (B) the sum of relative concentrations. The tree diagram on the top indicates the closeness between different *Jacobaea* plants. Different species are color coded as indicated in the right-most legend. Sn: the sum of senecionine-like PAs; Er: the sum of erucifoline-like PAs; Jb: the sum of jacobine-like PAs; Pt: the sum of platyphylline-like PAs; Ot: the sum of otosenine-like PAs; Unk: the sum of unknown PAs.

Fig. S13. Maximum likelihood ancestral state reconstruction of five PA structural groups and unknown PAs. The tree shown is the ML tree from the total plastid and nuclear dataset of 17 *Jacobaea* species. (A) senecionine-like group (B) erucifoline-like group (C) jacobine-like group (D) platyphylline-like group (E) otosenine-like group (F) unknown group. Character states were binary coded for each species taking each group of PAs as a unit and are shown as small pie charts before taxon names: black (presence) and white (absence). The pie charts shown at individual nodes illustrate the likelihood for the ancestral states.

Table S1. Primers used for amplification of plastid and nuclear DNA regions in 17 *Jacobaea* species and *S. vulgaris*.

Additional file S1. The full list of 80 pyrrolizidine alkaloids and data matrix used in statistical analyses.

Additional file S2. Ancestral state reconstruction of 80 pyrrolizidine alkaloids using the ML phylogeny.

Additional file S3. The phylogenetic signals of 80 pyrrolizidine alkaloids by K and λ statistics using the ML phylogeny.